

Seeing Topological Charges by Naked Eyes

Matheus S. M. de Sousa,¹ Antonio L. Cruz,¹ and Wei Chen¹

¹*Department of Physics, PUC-Rio, 22451-900 Rio de Janeiro, Brazil*

(Dated: March 28, 2023)

The opacity of graphene is known to be approximately given by the fine structure constant α times π . We point out the fact that the opacity is roughly independent of the frequency of the light can be attributed to the topological charge of the Dirac point. As a result, one can literally see the topological charge by naked eyes from the opacity of graphene, and moreover it implies that the fine structure constant is topologically protected. A similar analysis applied to 3D topological insulators suggests that their opacity in the infrared region is also given by $\pi\alpha$, which may be seen by naked eyes through an infrared lens, and ideally is independent of the thickness of the material since it is contributed solely from the topological surface states. For 3D Dirac or Weyl semimetals, the optical absorption power is linear to the frequency in the infrared region, with a linearity given by the fine structure constant and the topological charge of Weyl points.

Introduction.- A fundamentally important issue in the research of topological materials is how the topological order can be unambiguously detected in experiments. Conventionally, the most straightforward way is to detect the effects related to the metallic edge or surface states, such as the quantized Hall conductance[1, 2] or zero bias conductance[3], which only occur in topologically nontrivial phase and is directly determined by the bulk topological invariant. On the other hand, to our knowledge, there has yet been a bulk material property in the macroscopic scale that can be felt by human perception and be attributed to the topological order. This is in sharp contrast to the materials that possess Landau order parameters. For instance, magnetic order can be simply perceived from the force that repels or attracts two bar magnets, and superconductivity can be understood as the mechanism behind the magnetic levitation.

In this Letter, we point out that the topological charge of various materials containing gapless Dirac cones can actually be seen by naked eyes, either directly or through an infrared lens, owing to the optical absorption power that is proportional to the fine structure constant $\alpha = e^2/4\pi\hbar c\epsilon_0 \approx 1/137$ times a factor given by the topological charge \mathcal{C} . This feature originates from a correspondence between quantum geometry and topological order[4], and implies α can be extracted in a topologically protected manner from the frequency- or polarization-dependence of optical absorption in different materials. We will use several prototype topological materials including graphene, 3D topological insulators (TIs), and 3D Dirac and Weyl semimetals to explicitly demonstrate how α and \mathcal{C} appear in the optical absorption power, and then address how various factors in real materials, such as hexagonal warping, spin-orbit coupling, and many different sources of scattering can alter this simple picture, which nevertheless still serves as a pedagogical example to perceive the topological charge in the macroscopic scale.

Relating optical absorption power to quantum geometry.- Our survey starts by considering the quan-

tum geometry of valance band states[4–6]. We will reserve the index n for valance bands, m for conduction bands, ℓ for all the bands, and their energies at momentum \mathbf{k} are denoted by $\epsilon_{\ell}^{\mathbf{k}}$. For a gaped topological material with N_- valance bands, the fully antisymmetric valance band Bloch state at momentum \mathbf{k} is $|u^{\text{val}}(\mathbf{k})\rangle = \epsilon^{n_1 n_2 \dots n_{N_-}} |n_1\rangle |n_2\rangle \dots |n_{N_-}\rangle / \sqrt{N_-!}$. The quantum metric of this state is defined from[7]

$$|\langle u^{\text{val}}(\mathbf{k}) | u^{\text{val}}(\mathbf{k} + \delta\mathbf{k}) \rangle| = 1 - \frac{1}{2} g_{\mu\nu}(\mathbf{k}) \delta k^{\mu} \delta k^{\nu}, \quad (1)$$

whose diagonal component $g_{\mu\mu}$ can be calculated from each band by[4]

$$\begin{aligned} g_{\mu\mu}(\mathbf{k}) &= \langle \partial_{\mu} u^{\text{val}} | \partial_{\mu} u^{\text{val}} \rangle - \langle \partial_{\mu} u^{\text{val}} | u^{\text{val}} \rangle \langle u^{\text{val}} | \partial_{\mu} u^{\text{val}} \rangle \\ &= \sum_{nm} \langle \partial_{\mu} n | m \rangle \langle m | \partial_{\mu} n \rangle. \end{aligned} \quad (2)$$

To relate the quantum metric to optical responses, we introduce a quantum metric spectral function[6]

$$\begin{aligned} g_{\mu\mu}(\mathbf{k}, \omega) &= \sum_{\ell < \ell'} \langle \partial_{\mu} \ell | \ell' \rangle \langle \ell' | \partial_{\mu} \ell \rangle \\ &\times [f(\epsilon_{\ell}^{\mathbf{k}}) - f(\epsilon_{\ell'}^{\mathbf{k}})] \delta(\omega + \frac{\epsilon_{\ell}^{\mathbf{k}}}{\hbar} - \frac{\epsilon_{\ell'}^{\mathbf{k}}}{\hbar}) \\ &= \frac{V_D}{\pi e^2 \hbar \omega} \sigma_{\mu\mu}(\mathbf{k}, \omega), \end{aligned} \quad (3)$$

which at zero temperature frequency-integrates to the quantum metric $\lim_{T \rightarrow 0} \int_0^{\infty} d\omega g_{\mu\mu}(\mathbf{k}, \omega) = g_{\mu\mu}(\mathbf{k})$, where V_D is the volume of the D -dimensional unit cell, and $\sigma_{\mu\mu}(\mathbf{k}, \omega)$ is the finite temperature longitudinal optical conductivity at momentum \mathbf{k} [8].

The optical conductivity measured in real space is given by the momentum integration

$$\begin{aligned} \sigma_{\mu\mu}(\omega) &= V_D \int \frac{d^D \mathbf{k}}{(2\pi\hbar)^D} \sigma_{\mu\mu}(\mathbf{k}, \omega) \\ &= \frac{\pi e^2}{\hbar^{D-1}} \omega \int \frac{d^D \mathbf{k}}{(2\pi)^D} g_{\mu\mu}(\mathbf{k}, \omega) \equiv \frac{\pi e^2}{\hbar^{D-1}} \omega \mathcal{G}_{\mu\mu}(\omega), \end{aligned} \quad (4)$$

which defines what we call the fidelity number spectral function $\mathcal{G}_{\mu\mu}(\omega)$ [8]. Furthermore, applying an oscillating electric field polarized in μ direction $E_\mu(\omega, t) = E_0 \cos \omega t$ to the system induces a current that oscillates accordingly $j_\mu(\omega, t) = \sigma_{\mu\mu}(\omega) E_0 \cos \omega t$, where E_0 is the strength of the field. Thus the optical absorption power per unit cell at frequency ω is[8]

$$\begin{aligned} W_a^\mu(\omega) &= \langle j_\mu(\omega, t) E_\mu(\omega, t) \rangle_t = \frac{1}{2} \sigma_{\mu\mu}(\omega) E_0^2 \\ &= \frac{\pi e^2}{2\hbar^{D-1}} E_0^2 \omega \mathcal{G}_{\mu\mu}(\omega), \end{aligned} \quad (5)$$

where the time average gives $\langle \cos^2 \omega t \rangle_t = 1/2$. The main point of the present work is how $W_a^\mu(\omega)$ is related to the topological charge \mathcal{C} and fine structure constant α in a topologically protected manner, as we elaborate below for several different topological materials.

Opacity of pristine graphene.— The low energy band structure of graphene can be described by the tight-binding model on a honeycomb lattice with nearest-neighbor hopping $H = \sum_{\langle ij \rangle \sigma} t c_{i\sigma}^\dagger c_{j\sigma}$ with $t \approx 2.8\text{eV}$, and we denote the distance between neighboring carbon atoms by $a = 0.142\text{nm}$ [9]. For each spin species, the low energy Hamiltonian in the momentum space may be obtained by an expansion around the two Dirac points \mathbf{K} and \mathbf{K}' , yielding the linear Dirac Hamiltonian [10]

$$H_0^{\mathbf{K}, \mathbf{K}'}(\mathbf{k}) = v_F (\pm k_y \sigma_x - k_x \sigma_y), \quad (6)$$

where $v_F = 3ta/2\hbar$ is the Fermi velocity. This linearized model well describes the linear band structure up to energy $\sim 1\text{eV}$, and hence is a suitable model for the optical absorption in the visible light range. To proceed, we introduce the spin-valley index $\gamma = \{\mathbf{K} \uparrow, \mathbf{K} \downarrow, \mathbf{K}' \uparrow, \mathbf{K}' \downarrow\}$ and denote the valence and conduction band states by $|n^\gamma\rangle$ and $|m^\gamma\rangle$, whose eigenenergies $\varepsilon_n^{\mathbf{k}} = -v_F k$ and $\varepsilon_m^{\mathbf{k}} = v_F k$ do not depend on γ . The key point in our formalism is the relation between the topological charge $\mathcal{C} = 1/2$ and the azimuthal quantum metric $g_{\phi\phi}^\gamma = 1/4$ of any flavor γ [4, 11]

$$\begin{aligned} -\oint \frac{d\phi}{2\pi} \langle n^{\mathbf{K}\uparrow} | i\partial_\phi | n^{\mathbf{K}\uparrow} \rangle &= \oint \frac{d\phi}{2\pi} \langle n^{\mathbf{K}'\uparrow} | i\partial_\phi | n^{\mathbf{K}'\uparrow} \rangle \\ &= 1/2 \equiv \mathcal{C} = |\langle n^\gamma | i\partial_\phi | n^\gamma \rangle| = \sqrt{g_{\phi\phi}^\gamma}. \end{aligned} \quad (7)$$

Putting this result into Eq. (3) and (4), one obtains a fidelity number spectral function that contains a prefactor of \mathcal{C}^2

$$\mathcal{G}_{\mu\mu}(\omega) = \frac{\mathcal{C}^2}{\pi\omega} \left[f\left(-\frac{\hbar\omega}{2}\right) - f\left(\frac{\hbar\omega}{2}\right) \right]. \quad (8)$$

In addition, from Eq. (3), the optical conductivity contributed by the flavor γ is $\sigma_{\mu\mu}^\gamma(\mathbf{k}, \omega) = \pi e^2 \hbar \omega g_{\mu\mu}^\gamma(\mathbf{k}, \omega) / A_{\text{cell}}$, where $A_{\text{cell}} = 3\sqrt{3}a^2/2$ is the unit cell area of the hexagonal lattice, and hence the conductivity measured in real space is $\sigma_{\mu\mu}(\omega) =$

$\sum_\gamma \int \frac{d^2\mathbf{k}}{\hbar^2 A_{\text{BZ}}} \sigma_{\mu\mu}^\gamma(\mathbf{k}, \omega) = \frac{\pi e^2}{\hbar} \omega \mathcal{G}_{\mu\mu}(\omega)$, which links the optical conductivity of graphene[12, 13] to the spectral function $\mathcal{G}_{\mu\mu}(\omega)$, where $A_{\text{BZ}} = 8\pi^2/3\sqrt{3}a^2$ is the area of the BZ.

For an incident light with electric field E_0 , the incident power per unit cell of area A_{cell} is $W_i = c\varepsilon_0 E_0^2/2$. Using Eq. (5), the opacity at polarization μ and frequency ω is

$$\begin{aligned} \mathcal{O}(\omega) &= \frac{W_a^\mu(\omega)}{W_i} = 4\pi^2 \alpha \omega \mathcal{G}_{\mu\mu}(\omega) \\ &= \pi\alpha \times 4\mathcal{C}^2 \left[f\left(-\frac{\hbar\omega}{2}\right) - f\left(\frac{\hbar\omega}{2}\right) \right], \end{aligned} \quad (9)$$

which does not depend on the polarization μ . In the zero temperature limit, the Fermi factor drops out, so one obtains

$$\lim_{T \rightarrow 0} \mathcal{O}(\omega) = \pi\alpha \times 4\mathcal{C}^2 = \pi\alpha \approx 2.3\%. \quad (10)$$

This is the seminal result of the 2.3% opacity (or transmittance) of graphene[14–17], and our analysis brings in several new aspects to this result: (1) The independence of frequency ω is due to the topological charge $\mathcal{C} = 1/2$, or equivalently the azimuthal quantum metric $g_{\phi\phi}^\gamma$ according to Eq. (A4), that is independent of the circle of radius $k = \hbar\omega/2v_F$ at which the conduction band electrons are excited by the light. In addition, $g_{\phi\phi}^\gamma$ is also independent of the angle ϕ , hence the opacity does not depend on the polarization μ either. Since the visible light produced by common light sources usually contains a wide range of polarization and frequency, the reason that graphene always shows 2.3% opacity is due to the topological protection of the Dirac cone, and it implies that one can literally see the topological charge \mathcal{C} by naked eyes through the opacity. (2) One may use the plateau of frequency or polarization dependence of opacity to extract α . This procedure echoes the extraction of von Klitzing constant h/e^2 from the Hall plateaux as a function of magnetic field in the quantum Hall effect (QHE)[1], which is also topologically protected[18] (note that the magnetic field can also be converted into the cyclotron frequency). This topological protection implies that the measured α should be independent of many details of the system, i.e., ideally any 2D materials that have a Dirac code should have the same $\pi\alpha$ opacity, which may describe a variety of 2D materials such as graphynes[19, 20], B₂S[21], silicene[22–24], germanene[25], etc[26–28].

Despite this appealing connection between the opacity and topological charge, the above simple results suffer a great challenge from many realistic factors in 2D materials containing Dirac cones, as we formulate in the supplementary material and discuss below[11]. The first is the realistic band structure beyond the simple description of Eq. (6), which contains complications such as hexagonal warping and next-nearest-neighbor hopping. Investigating these effects by means of a tight-binding model leads us to conclude that the next-nearest-neighbor hopping

actually has no effect on either the opacity or the topological charge. However, the tight-binding band structure does feature an opacity that increases with frequency until the transition between van Hove singularities $\hbar\omega \approx 2t$, which makes the opacity in the visible light range to be $2.46\% < \mathcal{O}(\omega) < 2.71\%$, as has already been investigated theoretically and observed experimentally[14–17, 29, 30]. Nevertheless, since human eyes can hardly distinguish such a small deviation, the roughly $\approx 2.3\%$ opacity observed by human eyes can still serve as a pedagogical example to perceive the topological charge in graphene in the macroscopic scale. On the other hand, for 2D materials whose transition between van Hove singularities falls in the visible light range, such as silicene simulated by $t = 1.6\text{eV}$ [31] and shown in Fig. 1 (a), then the opacity will strongly depend on the color of the light. This result indicates that Dirac cone materials with larger hopping t , i.e., the linearity of Dirac cone extends beyond visible light range, are more ideal to visualize the topologically protected constant opacity. Nevertheless, because the opacity in the infrared region should still be $\pi\alpha$ for materials with a small t , the constant opacity may still be perceived by human eyes through an infrared lens. Finally, the finite temperature data in Fig. 1 (a) indicate that the thermal broadening in Eq. (9) only reduces the opacity in the low frequency region $\hbar\omega \lesssim k_B T$, which is far below and hence has negligible effect on the visible light range[15, 29].

Secondly, the realistic band structure also influences the polarization dependence of the opacity[11], yielding a 15% to 30% variation with the polarization angle ϕ_E in the visible light range, as shown in Fig. 1 (b). This variation is mainly contributed from the optical Hall conductance $\sigma_{xy}(\omega)$ originated from g_{xy} [11], and hence one can actually estimate the magnitude of $\sigma_{xy}(\omega)$ by simply rotating a graphene sheet against a polarized light and seeing how its opacity varies. However, this also indicates that it is hard to associate the opacity against a polarized light to the topological charge since it is not a constant of ϕ_E , and suggesting that only unpolarized light that averages over ϕ_E can serve this purpose.

Thirdly, for 2D materials that are not perfectly flat but have some buckling structure, the breaking of inversion symmetry can induce a Rashba spin-orbit coupling (RSOC). By incorporating the RSOC of strength λ_R into the honeycomb lattice[32], we obtain an opacity that shows an anomaly at frequency $\omega \sim 3\lambda_R$ owing to the splitting of the bands, as shown in Fig. 1 (c). Thus if the RSOC of some material happens to fall in the visible light region $1.8\text{eV} \lesssim 3\lambda_R \lesssim 3.1\text{eV}$, then its opacity may strongly depend on the color of the light. However, such a strong RSOC seems rather unlikely, since most of known 2D materials have an RSOC of the order of 10meV [33], and hence its influence on the visible light range is negligible.

Finally, concerning various sources of scattering,

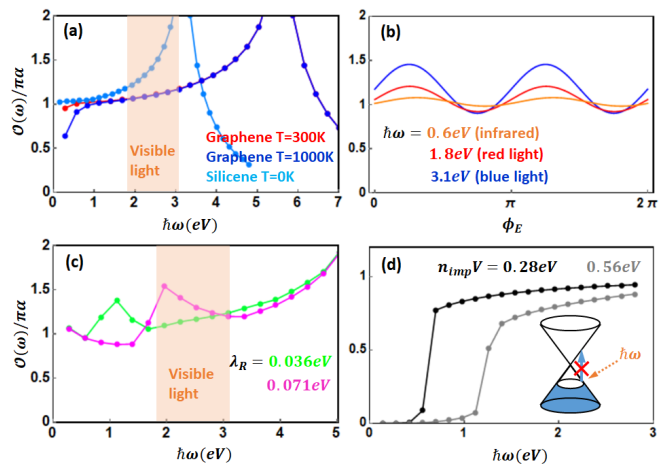


FIG. 1. (a) The opacity of graphene $\mathcal{O}(\omega)/\pi\alpha$ at $T = 300\text{K}$, 1000K (a rather unrealistic temperature just to demonstrate the effect), and silicene at $T = 0$ as a function of frequency of the unpolarized light. (b) The dependence of the opacity of graphene on the polarization angle ϕ_E at $T = 0$. (c) The effect of RSOC on the opacity of graphene at $T = 0$. (d) The effect of impurities on the opacity of linear Dirac model, with impurity density n_{imp} and strength V . The inset shows schematically how the energy shift caused by the real part of self-energy blocks the optical transition.

graphene under the influence of electron-electron interaction has been investigated intensively[34, 35], which only yields a very small correction to the opacity[36]. In contrast, we consider the effect of random point-like impurities[11, 37]. The results shown in Fig. 1 (d) indicate an opacity that is strongly suppressed in the low frequency regime $\hbar\omega \lesssim 2n_{imp}V$, which is caused by the real part of the self-energy that acts like a chemical potential, rendering the valence band states with energy less than $\epsilon_n^k < n_{imp}V$ empty. As a result, the optical absorption is strongly suppressed and hence the material actually becomes more transparent at $\hbar\omega \lesssim 2n_{imp}V$, as indicated by the inset of Fig. 1 (d). This suppression is in qualitative agreement with the experiment in fluorinated graphene, where a reduced low frequency opacity is observed, and the reduction region can be extended to the visible light range by increasing fluorine concentration[30]. In fact, changing the chemical potential should also cause such a suppression, as has been observed experimentally[38]. Thus to see the topological charge from the opacity in the visible light range, a clean and unbiased graphene is needed. Finally, we remark that the opacity is frequency-independent only if the topological material is gapless, as we demonstrate in the supplementary material using 2D Chern insulator as a counterexample[8, 11].

Opacity of 3D TIs. Interestingly, although 3D TIs like Bi_2Se_3 and Sb_2Te_3 have a bulk gap[39, 40], we predict that their opacity in the infrared region is also $\pi\alpha$ just like graphene owing to the gapless topological surface states. The bulk of 3D TI usually have a direct

band gap $2M \sim 0.5\text{eV}$, so in the topologically trivial phase it should have no optical absorption and hence ideally be transparent in the infrared region. However, in the topologically nontrivial phase, the TI has surface states in the top and bottom surfaces that the light passes through, each has two spin species, and hence one may label them by the four spin-surface flavors $\gamma = (\text{top } \uparrow, \text{top } \downarrow, \text{bottom } \uparrow, \text{bottom } \downarrow)$. Each γ is described by one of the Hamiltonians in Eq. (6) with a proper assignment of k_x and k_y [39–41], yielding the same opacity $\pi\alpha$ as graphene, and is also independent of the frequency and polarization in the infrared region owing to the topological charge of the surface state, equivalently the bulk topological invariant due to the bulk-edge correspondence. Moreover, the opacity should be independent of the thickness of the TI provided the material is thicker than the decay length of surface states (same as the correlation length $\hbar v_F/M \sim \text{nm}$ [42, 43]), and is the same for all 3D TIs with a direct band gap, which is ready to be verified by naked eyes through an infrared lens. Our result also implies that the opacity changes when the 3D TI undergoes a topological phase transition, which may help to detect the transition by optical means. Finally, we remark that the transmittance of Bi_2Se_3 grown on a relatively transparent fluorophlogopite mica has been measured, which however exhibits a rapid Fabry–Pérot oscillation with frequency[44], indicating that a free standing single-crystal 3D TI thin film may be necessary to obtain the constant $\pi\alpha$ opacity.

Optical absorption of 3D Dirac and Weyl semimetals.— We proceed to consider the low energy sector of type-I 3D Weyl semimetals, such as TaAs and TaP[45, 46], which contain pairs of Weyl points[47–49]. Their low energy eigenstates can be labeled by the valley index $\gamma = \{1, 2, \dots, N_W\}$, where N_W is the number of Weyl points. The Hamiltonian in the infrared region for each γ is well described by the Dirac model

$$H^\gamma(\mathbf{k}) = \pm(vk_x\sigma_x + vk_y\sigma_y + vk_z\sigma_z) = \pm\mathbf{d} \cdot \boldsymbol{\sigma}, \quad (11)$$

and we assume a cubic lattice of unit cell volume $V_D = a^3$ for simplicity. As detailed in the supplementary material[11], the absorption power summing over the three crystalline directions and then divided by the incident power per unit cell volume $W_i = c\varepsilon_0 E_0^2/2a$ yields

$$\begin{aligned} & \sum_{\mu=x,y,z} \frac{W_a^\mu(\omega)}{W_i} \\ &= \alpha|\mathcal{C}| \left(\frac{N_W a}{2v} \right) \omega \left[f\left(-\frac{\hbar\omega}{2}\right) - f\left(\frac{\hbar\omega}{2}\right) \right]. \quad (12) \end{aligned}$$

whose zero temperature limit is linear in frequency, as has been pointed out theoretically[50–53] and experimentally observed[54]. Our result further suggests that the optical absorption power summing over three crystalline directions is directly proportional to the module of the topological charge $|\mathcal{C}|$. In addition, since it

is proportional to the module, even if two Weyl nodes of opposite chirality merge together to form a Dirac semimetal[55, 56], the absorption power is still that described by Eq. (12), whose linearity in frequency has been observed experimentally[57]. Physically, this means that Dirac and Weyl semimetals appear darker under higher frequency light in the infrared region, which should be detectable by human eyes through an infrared lens, with a darkness given by the fine structure constant α , module of the topological charge $|\mathcal{C}|$, lattice constant a , Fermi velocity v , and the number of Weyl points N_W . Finally, we remark that 3D topological semimetals have surface states too, but since the bulk already absorbs light, the contribution from the surface states should be negligible in the bulk limit.

Conclusions.— In summary, we clarify that the approximate frequency-independence of the opacity of disorder-free and unbiased graphene can be attributed to the topological charge of Dirac points. In other words, the roughly $\pi\alpha \approx 2.3\%$ opacity of graphene against any sources of unpolarized visible light is a manifestation of topological charge. The same analysis applied to 3D TIs suggests that their opacity in the infrared region ideally is also the bulk topological invariant times $\pi\alpha$ independent of frequency, polarization, and thickness of the material. In contrast, for 3D Weyl and Dirac semimetals, the fine structure constant and topological charge also determine the linear dependence of optical absorption power on frequency. All these features suggest that the fine structure constant extracted from the opacity or optical absorption power of these materials is topologically protected, offering a very accessible way to estimate the constant in a topologically protected manner.

Appendix A: Detail of linear Dirac model calculation

For the linear Dirac model in Eq. (6) of the main text, the eigenstates of either spin, say spin up, do not depend on the module k but only on the polar angle ϕ of the momentum, and are given explicitly by

$$\begin{aligned} |n^{\mathbf{K}\uparrow}\rangle &= \frac{1}{\sqrt{2}} \begin{pmatrix} 1 \\ ie^{i\phi} \end{pmatrix}, & |m^{\mathbf{K}\uparrow}\rangle &= \frac{1}{\sqrt{2}} \begin{pmatrix} 1 \\ -ie^{i\phi} \end{pmatrix}, \\ |n^{\mathbf{K}'\uparrow}\rangle &= \frac{1}{\sqrt{2}} \begin{pmatrix} 1 \\ ie^{-i\phi} \end{pmatrix}, & |m^{\mathbf{K}'\uparrow}\rangle &= \frac{1}{\sqrt{2}} \begin{pmatrix} 1 \\ -ie^{-i\phi} \end{pmatrix} \end{aligned} \quad (A1)$$

and the expression is the same for spin \downarrow . The topological charge \mathcal{C} per spin at each of the two Dirac points \mathbf{K} and \mathbf{K}' is given by integrating the valence band Berry connection along a closed loop of radius k circulating the Dirac points

$$\begin{aligned} \oint \frac{d\phi}{2\pi} \langle n^{\mathbf{K}\uparrow} | i\partial_\phi | n^{\mathbf{K}\uparrow} \rangle &= - \oint \frac{d\phi}{2\pi} \langle n^{\mathbf{K}'\uparrow} | i\partial_\phi | n^{\mathbf{K}'\uparrow} \rangle \\ &= -1/2 \equiv -\mathcal{C}, \end{aligned} \quad (A2)$$

which has opposite signs at the two Dirac points.

We now elaborate the relation between this topological charge and the quantum metric, and how this relation eventually manifests in the opacity of graphene. The quantum metric for the valence band state of spin-valley flavor γ is defined from the overlap $|\langle n^\gamma(\mathbf{k})|n^\gamma(\mathbf{k}+\delta\mathbf{k})\rangle| = 1 - g_{\mu\nu}^\gamma \delta k^\mu \delta k^\nu / 2$. In particular, because $|n^\gamma\rangle$ in Eq. (A1) does not depend on the module k , the only nonzero component in the polar coordinates $\{\mu, \nu\} = \{k, \phi\}$ is the azimuthal component

$$g_{\phi\phi}^\gamma = |\langle m^\gamma | i\partial_\phi | n^\gamma \rangle|^2 = |\langle n^\gamma | i\partial_\phi | n^\gamma \rangle|^2 = \mathcal{C}^2 = \frac{1}{4}, \quad (\text{A3})$$

which is the same for all the four flavors of γ . Comparing with Eq. (A2), and use the fact that $\langle n^\gamma | i\partial_\phi | n^\gamma \rangle$ is a constant, one sees that the topological charge is actually given by the azimuthal quantum metric

$$\mathcal{C} = |\langle n^\gamma | i\partial_\phi | n^\gamma \rangle| = \sqrt{g_{\phi\phi}^\gamma}. \quad (\text{A4})$$

This relation, which has been called the metric-curvature correspondence, is the key to identify the opacity of graphene with the topological charge, as we shall see below.

The quantum metric in the Cartesian coordinates $\{\mu, \nu\} = \{x, y\}$ can be obtained from Eq. (A3) by utilizing $\partial_x = \cos\phi \partial_k - (\sin\phi/k)\partial_\phi$ and $\partial_y = \sin\phi \partial_k + (\cos\phi/k)\partial_\phi$. Moreover, because in the angular integration $\int_0^{2\pi} d\phi$ in the calculation of optical absorption below, the choice of $\phi = 0$ is arbitrary, so for any polarization $\mu = \{x, y\}$ we can simply set

$$g_{\mu\mu}^\gamma = \frac{\sin^2\phi}{k^2} g_{\phi\phi}^\gamma = \frac{\sin^2\phi}{k^2} \mathcal{C}^2. \quad (\text{A5})$$

It follows that the quantum metric spectral function in Eq. (3) of the main text for the flavor γ is

$$g_{\mu\mu}^\gamma(\mathbf{k}, \omega) = g_{\mu\mu}^\gamma [f(\varepsilon_n^{\mathbf{k}}) - f(\varepsilon_m^{\mathbf{k}})] \delta(\omega + \frac{\varepsilon_n^{\mathbf{k}}}{\hbar} - \frac{\varepsilon_m^{\mathbf{k}}}{\hbar}). \quad (\text{A6})$$

After a momentum integration and summation over γ , one obtains the fidelity number spectral function in Eq. (8) of the main text.

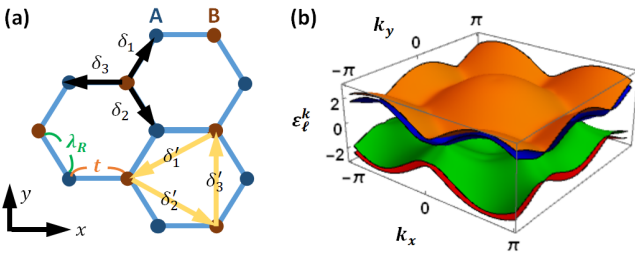


FIG. 2. (a) The definition of coordinates and various vectors on the honeycomb lattice. (b) The band structure simulated by $t = 1$, $t' = 0.036$, and $\lambda_R = 0.2$.

Appendix B: Effect of next-nearest-neighbor hopping and Rashba spin-orbit coupling

The effect of next-nearest-neighbor hopping and Rashba spin-orbit coupling (RSOC) may be investigated by incorporating them into the tight-binding model. For this purpose, we investigate the following model defined on a honeycomb lattice

$$H = -t \sum_{\langle ij \rangle, \sigma} c_{i\sigma}^\dagger c_{j\sigma} + t' \sum_{\langle\langle ij \rangle\rangle, \sigma} c_{i\sigma}^\dagger c_{j\sigma} + i\lambda_R \sum_{\langle ij \rangle, \alpha, \beta} c_{i\alpha}^\dagger (\boldsymbol{\sigma}_{\alpha\beta} \times \mathbf{d}_{ij})^z c_{j\beta}. \quad (\text{B1})$$

Here $c_{i\sigma}^\dagger$ ($c_{i\sigma}$) creates (annihilates) an electron of spin σ on the lattice site i , and $\langle ij \rangle$ and $\langle\langle ij \rangle\rangle$ indicate nearest-neighbor and next-nearest-neighbor lattice sites with the corresponding hopping $-t$ and t . The λ_R is the RSOC coupling constant, $\boldsymbol{\sigma} = (\sigma^x, \sigma^y, \sigma^z)$ are the spin Pauli matrices, \mathbf{d}_{ij} is the vector connecting the site i to j . Defining the basis $\psi = (A \uparrow, B \uparrow, A \downarrow, B \downarrow)$ and the Fourier transformation $c_{Ii\sigma} = \sum_{\mathbf{k}} e^{i\mathbf{k}\cdot\mathbf{r}_i} c_{I\mathbf{k}\sigma}$, where $I = \{A, B\}$ denotes the two sublattices and \mathbf{r}_i the unit cell position, the Hamiltonian $H = \sum_{\mathbf{k} I J \alpha \beta} c_{I\mathbf{k}\alpha}^\dagger H_{I\alpha J\beta}(\mathbf{k}) c_{J\mathbf{k}\beta}$ is described by the matrix

$$H_{I\alpha J\beta}(\mathbf{k}) = \begin{pmatrix} t'Z' & tZ^* & 0 & \lambda_R Y^* \\ tZ & t'Z' & \lambda_R X^* & 0 \\ 0 & \lambda_R X & t'Z' & tZ^* \\ \lambda_R Y & 0 & tZ & t'Z' \end{pmatrix},$$

$$Z \equiv e_1 + e_2 + e_3,$$

$$Z' \equiv e'_1 + e'_2 + e'_3,$$

$$X \equiv \frac{-1 - i\sqrt{3}}{2} e_1^* + \frac{-1 + i\sqrt{3}}{2} e_2^* + e_3^*,$$

$$Y \equiv \frac{1 + i\sqrt{3}}{2} e_1 + \frac{1 - i\sqrt{3}}{2} e_2 - e_3, \quad (\text{B2})$$

where the nearest neighbor $\boldsymbol{\delta}_a$ and next nearest neighbor vectors $\boldsymbol{\delta}'_a$ and the corresponding phase factors are

$$\boldsymbol{\delta}_1 = \left(\frac{1}{2}, \frac{\sqrt{3}}{2}\right), \quad \boldsymbol{\delta}_2 = \left(\frac{1}{2}, -\frac{\sqrt{3}}{2}\right), \quad \boldsymbol{\delta}_3 = (-1, 0),$$

$$\boldsymbol{\delta}'_1 = \left(-\frac{3}{2}, -\frac{\sqrt{3}}{2}\right), \quad \boldsymbol{\delta}'_2 = \left(\frac{3}{2}, -\frac{\sqrt{3}}{2}\right), \quad \boldsymbol{\delta}'_3 = (0, \sqrt{3}),$$

$$e_a = e^{i\mathbf{k}\cdot\boldsymbol{\delta}_a}, \quad e'_a = 2 \cos \mathbf{k} \cdot \boldsymbol{\delta}'_a, \quad (\text{B3})$$

These vectors and the resulting band structure using $t = 2.8\text{eV} \equiv 1$ as the energy unit, together with $t' = 0.1\text{eV} \equiv 0.036$ and $\lambda_R = 0.56\text{eV} \equiv 0.2$ (a rather large RSOC just to demonstrate the splitting of bands), are shown in Fig. 2. From the Hamiltonian matrix in Eq. (B2), one can calculate the velocity operators by $\hat{j}_\mu(\mathbf{k}) = e \partial_\mu H(\mathbf{k})$, which may then be used to calculate the optical conductivity and subsequently the quantum metric spectral function.

From the form of the Hamiltonian in Eq. (B2), one can immediately conclude that the next-nearest-neighbor hopping t' does not affect the quantum metric and opacity of graphene, simply because it enters the diagonal element of the Hamiltonian in the form of an identity matrix $t'Z' \times I_{4 \times 4}$. This means that t' does give a k -dependent deformation to the dispersion without modifying the eigenstates, and the deformation is the same for all the bands at \mathbf{k} and hence it does not affect the $\delta(\omega + \varepsilon_{\ell}^{\mathbf{k}}/\hbar - \varepsilon_{\ell'}^{\mathbf{k}}/\hbar)$ condition in the quantum metric spectral function either. As a result, the optical conductivity and opacity are not affected by t' .

Appendix C: Polarization dependence of opacity

To calculate the dependence of the direction of polarization $\hat{\boldsymbol{\mu}}$ of the light, we consider $\hat{\boldsymbol{\mu}}$ to be pointing at the polar angle ϕ_E on the xy -plane of graphene. The electric field and the corresponding current operator in this situation may be decomposed into

$$\begin{aligned} \mathbf{E} &= E_0 (\cos \phi_E \hat{\mathbf{x}} + \sin \phi_E \hat{\mathbf{y}}), \\ \hat{\mathbf{j}}_E &= \cos \phi_E \hat{j}_x + \sin \phi_E \hat{j}_y. \end{aligned} \quad (\text{C1})$$

The usual linear response theory requires to calculate the correlator $\langle [\hat{j}_E, \hat{j}_E] \rangle$, which yields an optical conductivity (suppressing (\mathbf{k}, ω))

$$\begin{aligned} \sigma_E &= \cos^2 \phi_E \sigma_{xx} + \sin^2 \phi_E \sigma_{yy} \\ &\quad + \sin \phi_E \cos \phi_E (\sigma_{xy} + \sigma_{yx}), \end{aligned} \quad (\text{C2})$$

which is equivalent to calculating the quantum metric (note that $g_{xy} = g_{yx}$)

$$\begin{aligned} g_E &= \cos^2 \phi_E g_{xx} + \sin^2 \phi_E g_{yy} \\ &\quad + 2 \sin \phi_E \cos \phi_E g_{xy}. \end{aligned} \quad (\text{C3})$$

The opacity will then carry the same angular dependence

$$\begin{aligned} \mathcal{O}_E(\omega, \phi_E) &= \cos^2 \phi_E \mathcal{O}_{xx}(\omega) + \sin^2 \phi_E \mathcal{O}_{yy}(\omega) \\ &\quad + 2 \sin \phi_E \cos \phi_E \mathcal{O}_{xy}(\omega), \end{aligned} \quad (\text{C4})$$

where $\mathcal{O}_{\mu\nu}(\omega)$ corresponds to the contribution coming from $g_{\mu\nu}$. Note that if a light source is not polarized, then averaging over the angle yields an opacity $\bar{\mathcal{O}}(\omega) = [\mathcal{O}_{xx}(\omega) + \mathcal{O}_{yy}(\omega)]/2$, meaning that the contribution from the off-diagonal element of the quantum metric g_{xy} drops out. However, for a polarized light, because $\mathcal{O}_{xx}(\omega) \approx \mathcal{O}_{yy}(\omega)$ (for instance,

$(\mathcal{O}_{xx}(\omega), \mathcal{O}_{yy}(\omega), \mathcal{O}_{xy}(\omega)) = (1.175, 1.182, 0.277) \times \pi\alpha$ for blue light $\hbar\omega = 3.1\text{eV}$), the variation of $\mathcal{O}_E(\omega, \phi_E)$ in Eq. (C4) as a function of the polarization angle ϕ_E mainly comes from the $2 \sin \phi_E \cos \phi_E \mathcal{O}_{xy}(\omega)$ term contributed from the optical Hall conductance $\sigma_{xy}(\omega)$, which is originated from the off-diagonal element of the quantum metric g_{xy} .

Appendix D: Effect of impurities

We proceed to utilize a many-body formalism to investigate the opacity of graphene under the influence of impurities. To give an analytical result at low energy, we adopt the spinless linear Dirac model of the basis $(c_{A\mathbf{k}}, c_{B\mathbf{k}})$ near the \mathbf{K} point as described by Eq. (6) of the main text, and consider the potential scattering

$$\hat{V} = V \begin{pmatrix} 1 & 0 \\ 0 & 1 \end{pmatrix}, \quad (\text{D1})$$

where V is the strength of impurity potential. We will focus on only one spin species near the \mathbf{K} valley, since all the four spin-valley flavors give the same result. The corresponding vertex for the $\ell = \{n, m\}$ band is

$$\begin{aligned} V_{\mathbf{k}\mathbf{k}'} &= \langle \ell\mathbf{k} | \hat{V} | \ell\mathbf{k}' \rangle = \langle n\phi | \hat{V} | n\phi' \rangle \\ &= \frac{V}{2} \left[1 + e^{i(\phi' - \phi)} \right], \end{aligned} \quad (\text{D2})$$

yielding the T -matrix for the ℓ band

$$\begin{aligned} T_{\mathbf{k}\mathbf{k}'}^{\ell}(\omega) &= \frac{V}{2} \left[1 + e^{i(\phi' - \phi)} \right] \sum_{s=0}^{\infty} \left(\frac{V}{2} \int \frac{k_1 dk_1}{2\pi/a^2} G_{\ell}(\mathbf{k}_1, \omega) \right)^s \\ &= \frac{\frac{V}{2} \left[1 + e^{i(\phi' - \phi)} \right]}{1 - \frac{V}{2} \int \frac{k_1 dk_1}{2\pi/a^2} G_{\ell}(\mathbf{k}_1, \omega)}. \end{aligned} \quad (\text{D3})$$

So we are lead to the integration of the retarded Green's function over the module of the momentum, assuming that it has a cut-off $0 < k_1 < \pi/a$

$$\begin{aligned} &\int_0^{\pi/a} \frac{k_1 dk_1}{2\pi/a^2} G_{\ell}(\mathbf{k}_1, \omega) \\ &= \int_0^{\pi/a} \frac{k_1 dk_1}{2\pi/a^2} \left[\frac{1}{\omega \pm vk} - i\pi\delta(\omega \pm vk) \right], \end{aligned} \quad (\text{D4})$$

where $+$ is for the valence band $\ell = n$ and $-$ is for the conduction band $\ell = m$, which leads to the result

$$\begin{aligned}
T_{\mathbf{k}\mathbf{k}'}^n(\omega) &= \frac{\frac{V}{2} \left[1 + e^{i(\phi-\phi')} \right]}{1 - \frac{Va^2}{4\pi v^2} \left[\frac{\pi v}{a} - \omega \ln \left| \frac{\pi v/a + \omega}{\omega} \right| \right] - i \frac{Va^2 \omega}{4v^2} \theta(0 > \omega > -\pi v/a)}, \\
T_{\mathbf{k}\mathbf{k}'}^m(\omega) &= \frac{\frac{V}{2} \left[1 + e^{i(\phi-\phi')} \right]}{1 - \frac{Va^2}{4\pi v^2} \left[-\frac{\pi v}{a} - \omega \ln \left| \frac{\pi v/a - \omega}{\omega} \right| \right] + i \frac{Va^2 \omega}{4v^2} \theta(0 < \omega < \pi v/a)},
\end{aligned} \tag{D5}$$

where the θ -function ensures the range of the frequency ω . The self-energy at momentum \mathbf{k} is simply the T -matrix at $\mathbf{k} = \mathbf{k}'$ multiplied by the density of the impurity $\Sigma_\ell(\mathbf{k}, \omega) = n_{imp} T_{\mathbf{k}\mathbf{k}}^\ell(\omega)$, which can be used to calculate the spectral function by

$$\begin{aligned}
A_\ell(\mathbf{k}, \omega) &= -\frac{1}{\pi} \text{Im} G_\ell(\mathbf{k}, \omega) \\
&= -\frac{1}{\pi} \frac{\text{Im} \Sigma_\ell(\mathbf{k}, \omega)}{(\omega \pm vk - \text{Re} \Sigma_\ell(\mathbf{k}, \omega))^2 + \text{Im} \Sigma_\ell(\mathbf{k}, \omega)^2}. \tag{D6}
\end{aligned}$$

After the spectral function is obtained, we further use the full Green's function approximation to obtain the dressed quantum metric spectral function $\tilde{g}_{\mu\nu}^\gamma(\mathbf{k}, \omega)$ for the spin-valley flavor γ by

$$\begin{aligned}
\tilde{g}_{\mu\nu}^\gamma(\mathbf{k}, \omega) &= \hbar g_{\mu\nu}^\gamma \int_{-\infty}^{\infty} d\varepsilon A_n(\mathbf{k}, \varepsilon) A_m(\mathbf{k}, \varepsilon + \hbar\omega) \\
&\quad \times [f(\varepsilon) - f(\varepsilon + \hbar\omega)] \tag{D7}
\end{aligned}$$

where $g_{\mu\nu}^\gamma$ is the unperturbed quantum metric. This dressed spectral function can then be used to calculate the opacity using the formalism presented in the main text. The spectral function $A_\ell(\mathbf{k}, \omega)$ shown in Fig. 3 exhibits a broadening of quasiparticle peak that gradually diminishes as $k \rightarrow 0$ owing to the imaginary part of self-energy, and a positive energy shift relative to the Dirac point of the pristine graphene due to the real part roughly given by the density of impurities times their strength $n_{imp}V$. This positive energy shift strongly suppresses the optical conductivity in the low frequency regime $\hbar\omega \lesssim 2n_{imp}V$, as argued in the main text.

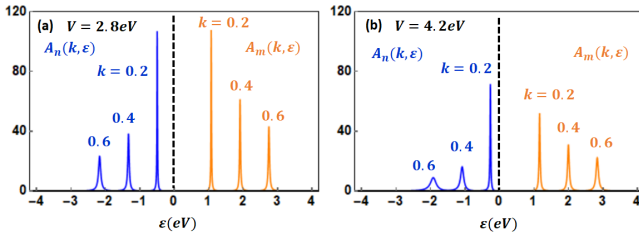


FIG. 3. Single-particle spectral function for the valence band $A_n(\mathbf{k}, \omega)$ and the conduction band $A_m(\mathbf{k}, \omega)$ of disordered graphene, where we fix the impurity density at $n_{imp} = 10\%$ and plot the results at impurity potential (a) $V = 0.28\text{eV}$ and (b) $V = 4.2\text{eV}$. The dashed line labels the Dirac point of the pristine graphene. The result suggests a shift of energy spectrum towards positive energy caused by the impurities.

Appendix E: Opacity of a Chern insulator

We remark that the constant opacity $\pi\alpha$ seems to manifest only if the unperturbed topological material is gapless. As a counter example, consider a 2D Chern insulator described by adding a mass term $M\sigma_z$ into the linear Dirac model in Eq. (6) of the main text, which gaps out the Dirac cone. The resulting fidelity number spectral function is

$$\begin{aligned}
\mathcal{G}_{\mu\mu}(\omega) &= \left[\frac{1}{16\pi\omega} + \frac{M^2}{4\pi\hbar^2\omega^3} \right] \\
&\quad \times \left[f\left(-\frac{\hbar\omega}{2}\right) - f\left(\frac{\hbar\omega}{2}\right) \right]_{\omega \geq 2|M|/\hbar} \tag{E1}
\end{aligned}$$

which yields an opacity that depends on the band gap M and is not a constant of frequency. Since the opacity depends on the color of the light and is not directly proportional to the Chern number, it is hard to argue that one can see the bulk topological invariant by naked eyes in this case.

Appendix F: Detail of the optical absorption power of Weyl semimetal

Starting from Eq. (11) of the main text, the topological charge of each Weyl point in a Weyl semimetal is calculated by the integration of Berry curvature over a spherical surface of any radius that encloses the Weyl point, whose sign depends on the chirality

$$\begin{aligned}
\mathcal{C} &= \pm \frac{1}{4\pi} \int d\phi \int d\theta \frac{1}{d^3} \varepsilon^{ijk} d_i \partial_\theta d_j \partial_\phi d_k \\
&= \pm \frac{1}{4\pi} \int d\phi \int d\theta \sin \theta = \pm 1, \tag{F1}
\end{aligned}$$

and we denote the integrand by $J_{\mathbf{k}} = \varepsilon^{ijk} d_i \partial_\theta d_j \partial_\phi d_k / d^3 = \sin \theta$. On the other hand, the quantum metric of each spin-valley flavor γ on the spherical surface is

$$g_{\theta\theta}^\gamma = \frac{1}{4}, \quad g_{\phi\phi}^\gamma = \frac{1}{4} \sin^2 \theta, \quad g_{\theta\phi}^\gamma = g_{\phi\theta}^\gamma = 0, \tag{F2}$$

which satisfies the metric-curvature correspondence

$$\sqrt{\det g^\gamma} = \frac{1}{4} |J_{\mathbf{k}}|. \tag{F3}$$

In the Cartesian coordinates, the metric is given by

$$g_{\mu\mu}^{\gamma} = \frac{1}{4k^4} (k^2 - k_{\mu}^2), \quad g_{\mu\nu}^{\gamma} |_{\mu \neq \nu} = -\frac{k_{\mu}k_{\nu}}{4k^4}. \quad (\text{F4})$$

and hence the trace of the quantum metric at \mathbf{k} for each spin-valley flavor $g_{xx}^{\gamma} + g_{yy}^{\gamma} + g_{zz}^{\gamma} = 1/2k^2$ only depends on the module k but not the direction $\hat{\mathbf{k}}$ of the momentum. As a result, using the definition of $g_{\mu\mu}^{\gamma}(\mathbf{k}, \omega)$ and $\mathcal{G}_{\mu\mu}(\omega)$ in the main text with $D = 3$, the conductivity in real space summing over three crystalline directions is

$$\begin{aligned} \sum_{\mu=x,y,z} \sigma_{\mu\mu}(\omega) &= \frac{N_W e^2 \omega}{4\pi \hbar^2} \left[\frac{1}{4\pi} \int d\phi \int d\theta \sin \theta \right] \\ &\times \int dk [f(-vk) - f(vk)] \frac{\hbar}{2v} \delta(k - \frac{\hbar\omega}{2v}) \\ &= \frac{N_W e^2 \omega |\mathcal{C}|}{8\pi \hbar v} \left[f\left(-\frac{\hbar\omega}{2}\right) - f\left(\frac{\hbar\omega}{2}\right) \right], \end{aligned} \quad (\text{F5})$$

since the bracket [...] in the second line is precisely the topological charge $|\mathcal{C}|$ in Eq. (F1). This averaged conductivity then yields the optical absorption power summing over three directions described by Eq. (12) of the main text.

-
- [1] K. v. Klitzing, G. Dorda, and M. Pepper, Phys. Rev. Lett. **45**, 494 (1980).
- [2] M. König, S. Wiedmann, C. Brüne, A. Roth, H. Buhmann, L. W. Molenkamp, X.-L. Qi, and S.-C. Zhang, Science **318**, 766 (2007).
- [3] V. Mourik, K. Zuo, S. M. Frolov, S. R. Plissard, E. P. A. M. Bakkers, and L. P. Kouwenhoven, Science **336**, 1003 (2012).
- [4] G. von Gersdorff and W. Chen, Phys. Rev. B **104**, 195133 (2021).
- [5] S. Matsuura and S. Ryu, Phys. Rev. B **82**, 245113 (2010).
- [6] W. Chen and G. von Gersdorff, SciPost Phys. Core **5**, 040 (2022).
- [7] J. P. Provost and G. Vallee, Comm. Math. Phys. **76**, 289 (1980).
- [8] M. S. M. de Souza, A. L. Cruz, and W. Chen, arXiv:2301.06493 (2023).
- [9] A. H. Castro Neto, F. Guinea, N. M. R. Peres, K. S. Novoselov, and A. K. Geim, Rev. Mod. Phys. **81**, 109 (2009).
- [10] B. A. Bernevig and T. L. Hughes, *Topological Insulators and Topological Superconductors* (Princeton University Press, 2013).
- [11] Supplementary material is given at:.
- [12] L. A. Falkovsky and A. A. Varlamov, EPJ B **56**, 281 (2007).
- [13] L. A. Falkovsky, J. Phys. Conf. Ser. **129**, 012004 (2008).
- [14] R. R. Nair, P. Blake, A. N. Grigorenko, K. S. Novoselov, T. J. Booth, T. Stauber, N. M. R. Peres, and A. K. Geim, Science **320**, 1308 (2008).
- [15] T. Stauber, N. M. R. Peres, and A. K. Geim, Phys. Rev. B **78**, 085432 (2008).
- [16] M. Bruna and S. Borini, Applied Physics Letters **94**, 031901 (2009).
- [17] J. W. Weber, V. E. Calado, and M. C. M. van de Sanden, Applied Physics Letters **97**, 091904 (2010).
- [18] D. J. Thouless, M. Kohmoto, M. P. Nightingale, and M. den Nijs, Phys. Rev. Lett. **49**, 405 (1982).
- [19] D. Malko, C. Neiss, F. Viñes, and A. Görling, Phys. Rev. Lett. **108**, 086804 (2012).
- [20] D. Malko, C. Neiss, and A. Görling, Phys. Rev. B **86**, 045443 (2012).
- [21] Y. Zhao, X. Li, J. Liu, C. Zhang, and Q. Wang, J. Phys. Chem. Lett. **9**, 1815 (2018).
- [22] M. Ezawa, Phys. Rev. Lett. **110**, 026603 (2013).
- [23] M. Houssa, A. Dimoulas, and A. Molle, J. Phys. Condens. Matter **27**, 253002 (2015).
- [24] S. Sadeddine, H. Enriquez, A. Bendounan, P. Kumar Das, I. Vobornik, A. Kara, A. J. Mayne, F. Sirotti, G. Dujardin, and H. Oughaddou, Sci. Rep. **7**, 44400 (2017).
- [25] A. Acun, L. Zhang, P. Bampoulis, M. Farmanbar, A. van Houselt, A. N. Rudenko, M. Lingenfelder, G. Brocks, B. Poelsema, M. I. Katsnelson, and H. J. W. Zandvliet, J. Phys. Condens. Matter **27**, 443002 (2015).
- [26] T. Wehling, A. Black-Schaffer, and A. Balatsky, Adv. Phys. **63**, 1 (2014).
- [27] S. Balendhran, S. Walia, H. Nili, S. Sriram, and M. Bhaskaran, Small **11**, 640 (2015).
- [28] J. Wang, S. Deng, Z. Liu, and Z. Liu, Natl. Sci. Rev. **2**, 22 (2015).
- [29] A. B. Kuzmenko, E. van Heumen, F. Carbone, and D. van der Marel, Phys. Rev. Lett. **100**, 117401 (2008).
- [30] R. R. Nair, W. Ren, R. Jalil, I. Riaz, V. G. Kravets, L. Britnell, P. Blake, F. Schedin, A. S. Mayorov, S. Yuan, M. I. Katsnelson, H.-M. Cheng, W. Strupinski, L. G. Bulusheva, A. V. Okotrub, I. V. Grigorieva, A. N. Grigorenko, K. S. Novoselov, and A. K. Geim, Small **6**, 2877 (2010).
- [31] M. Ezawa, Journal of the Physical Society of Japan **84**, 121003 (2015).
- [32] M. S. M. de Sousa, M. Sigrist, and W. Chen, Phys. Rev. Res. **3**, 033021 (2021).
- [33] C.-C. Liu, H. Jiang, and Y. Yao, Phys. Rev. B **84**, 195430 (2011).
- [34] I. F. Herbut, V. Juričić, and O. Vafek, Phys. Rev. Lett. **100**, 046403 (2008).
- [35] D. C. Elias, R. V. Gorbachev, A. S. Mayorov, S. V. Morozov, A. A. Zhukov, P. Blake, L. A. Ponomarenko, I. V. Grigorieva, K. S. Novoselov, F. Guinea, and A. K. Geim, Nat. Phys. **7**, 701 (2011).
- [36] D. E. Sheehy and J. Schmalian, Phys. Rev. B **80**, 193411 (2009).
- [37] T. Ando, Y. Zheng, and H. Suzuura, Journal of the Physical Society of Japan **71**, 1318 (2002).
- [38] Z. Q. Li, E. A. Henriksen, Z. Jiang, Z. Hao, M. C. Martin, P. Kim, H. L. Stormer, and D. N. Basov, Nat. Phys. **4**, 532 (2008).
- [39] H. Zhang, C.-X. Liu, X.-L. Qi, X. Dai, Z. Fang, and S.-C. Zhang, Nat. Phys. **5**, 438 (2009).
- [40] C.-X. Liu, X.-L. Qi, H. Zhang, X. Dai, Z. Fang, and S.-C. Zhang, Phys. Rev. B **82**, 045122 (2010).
- [41] X.-L. Qi and S.-C. Zhang, Rev. Mod. Phys. **83**, 1057 (2011).
- [42] W. Chen, M. Legner, A. Rüegg, and M. Sigrist, Phys. Rev. B **95**, 075116 (2017).
- [43] W. Chen and A. P. Schnyder, New J. Phys. **21**, 073003 (2019).

- [44] H. Peng, W. Dang, J. Cao, Y. Chen, D. Wu, W. Zheng, H. Li, Z.-X. Shen, and Z. Liu, *Nat. Chem.* **4**, 281 (2012).
- [45] H. Weng, C. Fang, Z. Fang, B. A. Bernevig, and X. Dai, *Phys. Rev. X* **5**, 011029 (2015).
- [46] H. Huang, Z. Liu, H. Zhang, W. Duan, and D. Vanderbilt, *Phys. Rev. B* **92**, 161115 (2015).
- [47] B. Yan and C. Felser, *Annu. Rev. Condens. Matter Phys.* **8**, 337 (2017).
- [48] N. P. Armitage, E. J. Mele, and A. Vishwanath, *Rev. Mod. Phys.* **90**, 015001 (2018).
- [49] B. Q. Lv, T. Qian, and H. Ding, *Rev. Mod. Phys.* **93**, 025002 (2021).
- [50] P. Hosur, S. A. Parameswaran, and A. Vishwanath, *Phys. Rev. Lett.* **108**, 046602 (2012).
- [51] A. Bácsı and A. Virosztek, *Phys. Rev. B* **87**, 125425 (2013).
- [52] T. Timusk, J. P. Carbotte, C. C. Homes, D. N. Basov, and S. G. Sharapov, *Phys. Rev. B* **87**, 235121 (2013).
- [53] P. E. C. Ashby and J. P. Carbotte, *Phys. Rev. B* **89**, 245121 (2014).
- [54] B. Xu, Y. M. Dai, L. X. Zhao, K. Wang, R. Yang, W. Zhang, J. Y. Liu, H. Xiao, G. F. Chen, A. J. Taylor, D. A. Yarotski, R. P. Prasankumar, and X. G. Qiu, *Phys. Rev. B* **93**, 121110 (2016).
- [55] S. M. Young, S. Zaheer, J. C. Y. Teo, C. L. Kane, E. J. Mele, and A. M. Rappe, *Phys. Rev. Lett.* **108**, 140405 (2012).
- [56] J. L. Mañes, *Phys. Rev. B* **85**, 155118 (2012).
- [57] R. Y. Chen, S. J. Zhang, J. A. Schneeloch, C. Zhang, Q. Li, G. D. Gu, and N. L. Wang, *Phys. Rev. B* **92**, 075107 (2015).